Ⅲ-3

Chemistry

Highlight

BL1U

Limitations in Photoionization of Helium by an Extreme Ultraviolet Vortex

T. Kaneyasu[1], Y. Hikosaka[2], M. Fujimoto[3], M. Katoh[3], H. Iwayama[3] and E. Shigemasa[3]

[1]*SAGA Light Source, Tosu 841-0005, Japan*

[2]*Graduate School of Medicine and Pharmaceutical Sciences, University of Toyama, Toyama 930-0194, Japan*

[3]*UVSOR Facility, Institute for Molecular Science, Okazaki 444-8585, Japan*

We report the experimental investigation on the photoionization of helium atoms irradiated with a circularly polarized extreme ultraviolet (XUV) vortex beam produced by a helical undulator [1]. The XUV vortex has a helical wavefront and carries orbital angular momentum (OAM) as well as spin angular momentum associated with it circular polarization. In recent years, several theoretical works have been reported on the photoionization and photoexcitation of atoms by OAM-carrying photons [2]. Differing from plane-wave photons, a violation of the standard electric dipole selection rules is predicted for vortex, as a consequence of the transference of the OAM to the internal degrees of freedom of the atom. In contrast to these advances in theory, to our knowledge, there has been no experimental work on vortex-matter interactions in the short wavelength regime, owing to the technical difficulty of producing brilliant and energy-tunable vortex beams.

The experiment was carried out at the undulator beamline BL1U. The experimental setup is shown in Fig. 1. The XUV vortex beams at about 30 eV photon energy were produced by a helical undulator as the higher harmonics of its radiation because the *n*th harmonic off-axis radiation from a helical undulator carries OAM of $(n-1)\hbar$ per photon [3, 4], as a result of the spiral motion of electron which naturally emits electromagnetic wave with a helical wavefront [5]. To avoid possible distortions of the helical wave front characterizing the XUV vortex, we did not use any optical elements in the experiment. The interaction point was placed at about 11 m downstream from the undulator, where the sample gas was admitted from an aperture. The central part of the undulator radiation was cut out by a 1-mm-diameter pinhole. Photoelectron angular distributions of helium atoms were measured by using a velocity map imaging (VMI) spectrometer.

Figure 2 shows the angular distributions measured for the first, second and third harmonics, corresponding to plane-wave photons (l=0), and XUV vortices of l=1 and 2, respectively. While the violation of the electric dipole transition rules has been predicted for interactions between vortices and atoms, the photoelectron angular distributions are well reproduced by the dipole components alone, and non-dipole contributions are not detected within the experimental uncertainty. This observation can be explained by considering the localized nature of the helical phase effect of the vortex on the interaction with atoms, and demonstrates that non-dipole interactions induced by vortex are hardly observable in conventional gas-phase experiments.

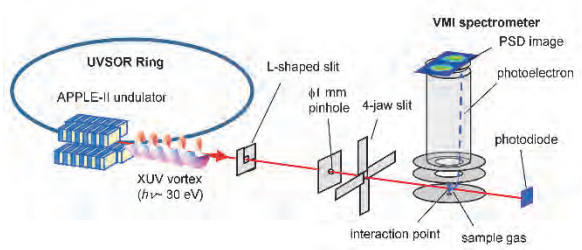

Fig. 1. Experimental setup used for photoionization experiment of helium atoms by the XUV vortex. The XUV vortex produced by the APPLE-II undulator is introduced into the interaction point without any optical elements.

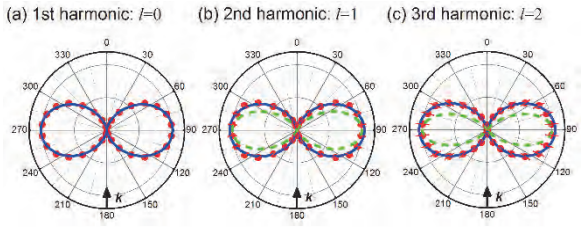

Fig. 2. Photoelectron angular distributions of helium atoms measured for the (a) first, (b) second and (c) third harmonics from helical undulator. The solid blue curves represent fits assuming electric dipole transition. The dotted green curves in (b) and (c) show the angular dependence of the photoelectron expected for non-dipole transitions induced by the OAM carried by the XUV vortex.

[1] T. Kaneyasu *et al*., Phys. Rev. A **95** (2017) 023413.
[2] A. Picón *et al*., New J. Phys. **12** (2010) 083053.
[3] S. Sasaki and I. McNulty, Phys. Rev. Lett. **100** (2008) 124801.
[4] J. Bahrdt *et al*., Phys. Rev. Lett. **111** (2013) 034801.
[5] M. Katoh *et al*., Phys. Rev. Lett. **118** (2017) 094801.

BL1U

Optical Vortex or Polarized UV Light Induced Supramolecular Chiral Orientation of an Achiral Metal Complex in a Soft Polymer Matrix

M. Takase[1], T. Akitsu[1] and M. Katoh[2]

[1]*Department of Chemistry, Faculty of Science, Tokyo University of Science, Tokyo 162-8601, Japan*

[2]*UVSOR Facility, Institute for Molecular Science, Okazaki 444-8585, Japan*

It is well known that a lot of organic polymers of liquid crystals containing azo-groups exhibit optical anisotropy after polarized UV light irradiation (Weigert effect). In recent years, we have systematically investigated organic/inorganic hybrid materials composed of chiral Schiff base metal complexes and azo-compounds in PMMA polymer films [1], chiral Schiff base metal complexes without azo-groups in protein matrix [2], and achiral Schiff base metal complex without azo-group in PVA polymer film [3] to discuss induced optical anisotropy after linearly polarized UV light irradiation or induced chiral supramolecular arrangement after circularly UV light irradiation.

In this time, we prepared organic/inorganic hybrid materials composed of water soluble binuclear Zn(II) Schiff base complex (Zn2L) without azo-compound in a PVA film to investigate not only linearly or circularly polarized UV light induced molecular orientation but also optical vortex UV light induced molecular orientation or changes by means of UVSOR BL1U.

As shown in Fig. 1, we have synthesized and characterized new Schiff base dinuclear Zn(II) complex involving chroride axial ligands and also prepared PVA polymer cast films. Without photochrmoic additives, optical dichroism at charge transfer bands could be observed after linearly polarized UV light irradiation with electric field vector of polarization due to increasing anisotropy of molecular orientation of the complexes directly. For example, the related Ni(II) complex most clearly exhibited anisotropy after linearly polarized UV light irradiation for 10 min. Fig. 2 exhibits angular dependence of polarized UV-vis spectra (absorbance at 367 nm) of Ni(II) complex. The Zn(II) complex also indicated similar behavior to Ni(II) one.

Comparing with several CD data of control experiments (only PVA film or hybrid materials, solutions or film, wavelengths or orbital angular moment dependence of UV light), we could derive preliminary results that optical vortex or polarized UV light (Fig. 3) induced molecular orientation of the Zn(II) complex in hybrid materials.

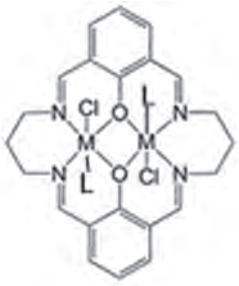

Fig. 1. Molecular structure of Zn(II) complex.

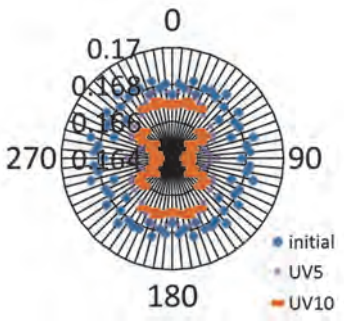

Fig. 2. Angular dependence of polarized UV-vis spectra (367 nm) of Ni(II) complex in PVA film after linearly polarized UV light irradiation (< 350 nm).

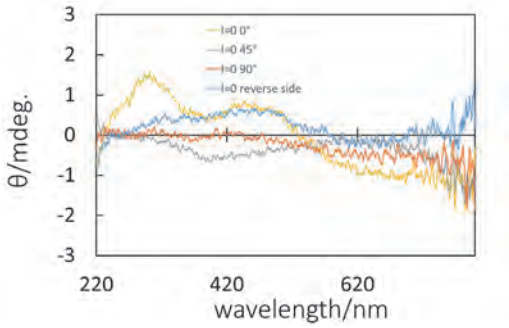

Fig. 3. CD spectra of of Zn(II) complex in PVA film after optical vortex (l=0) UV light irradiation (380 nm).

[1] N. Sunaga, C. Kominato, N. Ishida, M. Ito, T. Akitsu, T. Konomi and M. Katoh, *Azobenzene: Aspects, Applications and Reserach* (Nova Science Publishers, Inc., New York, 2017).

[2] E. Tsuda, Y. Mitsumoto, K. Takakura, N. Sunaga, T. Akitsu, T. Konomi and M. Katoh, J. Chem. Chem. Eng. **2** (2016) 53.

[3] M. Takase and T. Akitsu, *Polymers Book Series #1: Polymer science: research advances, practical applications and educational aspects* (Formatex Research Center, Badajoz (Spain), 2016).

BL3U

Local Structure of Crown Ether Inclusion Complex in Water by Soft X-ray Absorption Spectroscopy I. Interaction between Crown Ether and Ca^{2+}

H. Yuzawa, M. Nagasaka and N. Kosugi
Institute for Molecular Science, Okazaki 444-8585, Japan

Since the interaction in inclusion complexes shows a crucial role for life phenomena etc. but is not investigated in detail with conventional spectroscopic analysis [1], new methodologies are still required for detailed analysis of the interaction. Our research group has developed a liquid cell for the soft X-ray XAS in the transmission mode and has applied it to measurements of various aqueous solutions [2]. In the present study, we have extended this method to the measurement for the inclusion complex system of crown ethers in water to observe the interaction. Especially, we paid attention to the influence of the pore diameter of crown ether on the interaction in inclusion complexes by using three different crown ethers. In this part, we report Ca L-edge XAS of aqueous $Ca(SCN)_2$ crown ether solutions.

The experiments were carried out at BL3U. Aqueous solution samples (molar ratio, $Ca(SCN)_2$: H_2O = 1 : 59, $Ca(SCN)_2$: H_2O : 18-crown-6 = 1 : 59 : 1, $Ca(SCN)_2$: H_2O : 15-crown-5 = 1 : 59 : 1 and $Ca(SCN)_2$: H_2O : 12-crown-4 = 1 : 195 : 1) were prepared by using the commercial reagents without further purification. After the liquid cell which is composed of two Si_3N_4 membranes was filled with the liquid sample, the thickness (absorbance) of liquid samples was optimized by controlling the He pressure around the cell and then the Ca L-edge XAS was measured. The photon energy was calibrated by using the C K-edge XAS spectrum of the proline thin layer.

Figure 1 shows the obtained Ca L-edge XAS spectra. Two intense absorption peaks are assigned to Ca $2p_{3/2}$ → 3d excitation around 349.3 eV and Ca $2p_{1/2}$ → 3d one around 352.6 eV. These peak energies are slightly shifted to the lower energy (orange, green and blue lines in inset figures) compared with that in the simple aqueous $Ca(SCN)_2$ solution (red line). On the other hand, in the case of aqueous $Ca(SCN)_2$-EtOH solution (molar ratio, $Ca(SCN)_2$: H_2O : EtOH = 1 : 59 : 3), the energy shift is not observed (data not shown). This result indicates that the observed energy shift arises from the formation of crown ether-Ca^{2+} inclusion complex.

In the lower energy regions for the intense peaks, fine absorption structures in weak intensity are observed (Fig. 1, upper figure) mainly because the crystal field splitting of 3d states [3]. In the 18-crown-6 contained solution (orange line), the shapes of peaks around 348.4 and 351.4 eV is clearly different from the other samples. Compared with the previous report for the Ca L-edge spectra of solid CaF_2, the obtained difference is similar to the change for the coordinative unsaturation (disordered coordination symmetry) [4]. In addition, the pore diameter of 18-crown-6 is larger than the ionic diameter of Ca^{2+} (1.98 Å), whose size is fitted for that of 15-crown-5. Thus, Ca^{2+} would be coordinated by 18-crown-6 more unsymmetrically than the other samples with its molecular frame folding. In the 15-crown-5 contained sample (green line), the peak shape around 351.6 eV is more symmetrical than the other samples. This may be because the coordination symmetry is the highest in the samples [4].

Therefore, Ca L-edge XAS can be used as an effective indication of the coordination symmetry of crown ether complexes.

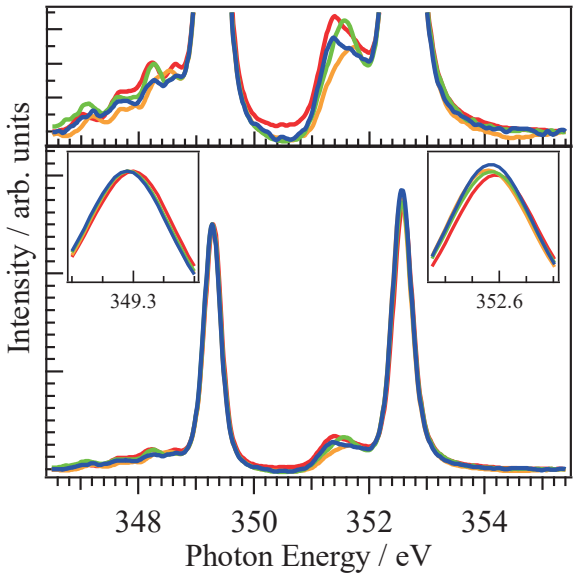

Fig. 1. Ca L-edge soft x-ray absorption spectra of aqueous $Ca(SCN)_2$ solution (red line), that containing 18-crown-6 (orange line), that containing 15-crown-5 (green line) and that containing 12-crown-4 (blue line). Upper figure is magnified view of small peaks and two inset figures are magnified views of two intense absorption (Ca-L_3 and L_2) peaks.

[1] G.W. Gokel, W.M. Leevy and M.E. Weber, Chem. Rev. **104** (2004) 2723.
[2] M. Nagasaka, H. Yuzawa and N. Kosugi, J. Spectrosc. Relat. Phenom. **200** (2015) 293.
[3] M.F.M. de Groot *et al*., Phys. Rev. B **41** (1990) 928.
[4] M.F.M. de Groot *et al*., Phys. Rev. B **43** (1991) 6899.

BL3U

Local Structure of Crown Ether Inclusion Complex in Water by Soft X-ray Absorption Spectroscopy II. Interaction between Crown Ether-Ca^{2+} Complex and SCN^- Anion

H. Yuzawa, M. Nagasaka and N. Kosugi
Institute for Molecular Science, Okazaki 444-8585, Japan

It is shown in Part I that the Ca L-edge XAS spectra of $Ca(SCN)_2$-crown ether solutions can give the information about the coordination symmetry of crown ether-Ca^{2+} inclusion complexes [1]. In this Part II, we show C K-edge and N K-edge XAS spectra for SCN^- anion to investigate the interaction between crown ether-Ca^{2+} inclusion complex and SCN^- anion.

The experiments were carried out at BL3U. The procedure of the XAS measurement is the same as that in Part I [1]. Another aqueous solution ($Ca(SCN)_2$: H_2O : EtOH = 1 : 59 : 3) was also prepared. In N K-edge XAS, a liquid cell composed of two SiC membranes instead of Si_3N_4 was used. The photon energy was calibrated by using C K-edge and N K-edge XAS spectra of the proline thin layer.

Figure 1 (a) shows the obtained N K-edge XAS spectra. The absorption peak around 399.5 eV is assigned to the 1s → π* excitation of SCN^- anion, whose peak top energy is constant regardless of the addition of the crown ethers. In the previous report of KSCN aggregate structure in aqueous solution, the N atom in SCN^- interacts with K^+ and the N K-edge peak top energy is shifted to the lower energy than that of hydrated SCN^- [2]. Thus, the constant absorption peak energy for the Ca(SCN)-crown ether solutions would be because N atom in SCN^- is apart from crown ether-Ca^{2+} complex.

Figures 1 (b) and (c) show C K-edge XAS spectra. The obtained peak around 287.3 eV is assigned to the 1s → π* excitation of SCN^- anion. The peak energy is shifted to the lower energy (Fig. 1 (b), orange, green and blue lines) compared with that in the simple aqueous $Ca(SCN)_2$ solution (red line), while in the case of aqueous $Ca(SCN)_2$-EtOH solution, the energy shift is not observed (Fig. 1 (c), gray line). This indicates that crown ether-Ca^{2+} inclusion complex and SCN^- anion are not completely dissociated and are interacted with each other. However, in the case of KSCN aqueous solution, the peak energy of C K-edge XAS in SCN^- is constant without relation to the formation of aggregate structures, which means that the C atom in SCN^- hardly interacts with cations [2]. Furthermore, peak energy shift is not induced by EtOH without the coordination to Ca^{2+} (Fig. 1 (c), grey line). Thus, the obtained energy shift would arise from the interaction between the C atom in SCN^- and crown ether ligand.

Therefore, the interaction between crown ether-Ca^{2+} inclusion complex and SCN^- is expected as follows. The coordination of crown ether to Ca^{2+} induces the interaction between Ca^{2+} and SCN^- from the S atom direction. In this structure, the C atom is close to (interacted with) the crown ether ligand to induce the energy shift of C K-edge XAS.

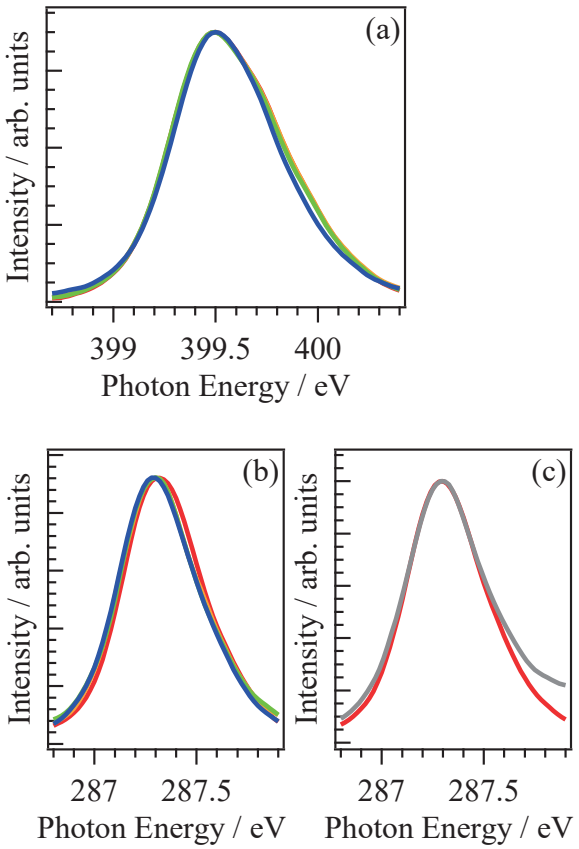

Fig. 1. (a) N K-edge XAS spectra of aqueous $Ca(SCN)_2$ solution (red line), that containing 18-crown-6 (orange line), that containing 15-crown-5 (green line) and that containing 12-crown-4 (blue line), (b) C K-edge XAS spectra for the same solutions as those of (a) and (c) C K-edge XAS of aqueous $Ca(SCN)_2$ solution (red line) and that containing EtOH (gray line). The deviation in higher energy region (> 287.5 eV) between red line and gray line is derived from the absorption of EtOH.

[1] H. Yuzawa, M. Nagasaka and N. Kosugi, UVSOR Activity Report in this volume.
[2] H. Yuzawa, M. Nagasaka and N. Kosugi, UVSOR Activity Report **42** (2015) 97.

BL3U

Study of Salting Effects in Compounds with Atmospheric Relevance by Using Soft X-ray Absorption Spectroscopy

G. Michailoudi[1], M. Patanen[1], N. Prisle[1], M. Huttula[1], H. Yuzawa[2], M. Nagasaka[2] and N. Kosugi[2]
[1]*Nano and Molecular Systems research unit, University of Oulu, P.O. Box 3000, 90014 University of Oulu, Finland*
[2]*UVSOR Synchrotron, Institute for Molecular Science, Okazaki 444-8585, Japan*

The aerosol particles in the atmosphere have an important effect on climate. Previous studies revealed the great impact of interactions between organic and inorganic compounds on atmospheric chemistry [1, 2]. In order to study salting effects on atmospheric organics, soft X-ray absorption spectroscopy was applied. This method has the advantage of high sensitivity to the chemical environment of the absorbing atom and together with molecular dynamics / quantum mechanics modelling our aim is to learn i) what are the structures of the formed hydrates of these organics ii) what are the relative concentrations of hydrated forms iii) how addition of salts changes the relative abundance of the hydrates and does e.g. ion-pairing or complex formation occur.

Aqueous solutions of organic compounds glyoxal ($C_2H_2O_2$), methylglyoxal ($C_3H_4O_2$), and glycerol ($C_3H_8O_3$) were prepared in the chemistry laboratory right before the experiments, in different concentrations, ranging from 0.1 to 2 M. These compounds were also mixed with sodium chloride (NaCl) or sodium sulfate (Na_2SO_4), with different mixing ratios, while the concentrations of salts were 1 and 2 M. The samples were placed to a liquid flow cell [3] and exposed to soft X-ray radiation at BL3U beamline at UVSOR synchrotron. In order to investigate the carbon K-edge absorption spectra, the photon energy was scanned between 280 and 305 eV, and for the oxygen K-edge absorption spectra, the chosen photon energy range was from 525 to 550 eV.

Figure 1 presents examples of the preliminary analysed data at the C 1s absorption edge of binary glyoxal - water and methyl glyoxal – water solutions (black and red circles, respectively) together with Na_2SO_4 addition. A background spectrum containing absorption from water and liquid cell membranes has been subtracted. The addition of salt does not introduce shifts to the observed absorption features and it can be concluded that in case of glyoxal, the bihydrated form is dominating. Methyl glyoxal shows three distinct absorption features which can be associated with its three inequivalent carbons.

Figure 2 shows a comparison of 2 M glyoxal solution (purple), 2 M Na_2SO_4 solution (green) and their mixture (red), together with a water spectrum (dashed blue line). The spectra have been normalized to the background preceding the water pre-peak. The pre-peak shifts upon addition of Na_2SO_4, which is evident from pure Na_2SO_4 aqueous solution. Modelling is needed to further conclude about the aqueous forms of the studied organics.

The obtained data will give valuable information of bulk properties of these solutions, as in larger framework we are interested in the interactions occurring in clusters and aerosols containing these compounds, their physical and chemical properties and their reactivity. Our goal is to access the missing molecular scale information of aerosol particles and to better understand their impact on climate.

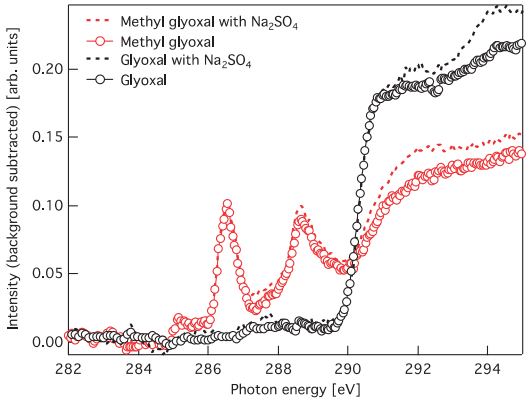

Fig. 1. C K-edge spectra of glyoxal – water (2 M) and methyl glyoxal - water (1 M) binary solutions and 1 : 1 mixtures with Na_2SO_4.

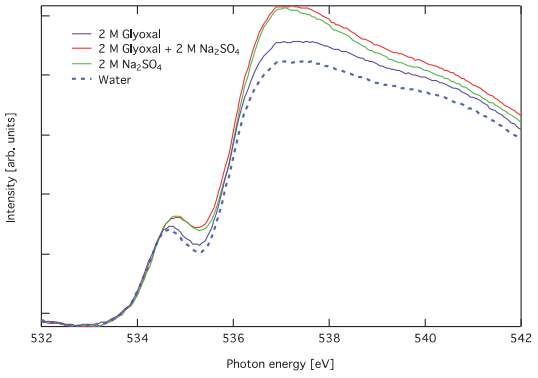

Fig. 2. A comparison of 2 M aqueous solution of glyoxal, 2 M Na_2SO_4 solution and their mixture, together with a water spectrum.

[1] T. Kurtén *et al.*, J. Phys. Chem. A **119** (2015) 4509.
[2] A.M.K. Hansen *et al.*, Atmos. Chem. Phys. **15** (2015) 14071.
[3] M. Nagasaka, T. Hatsui, T. Horigome, Y. Hamamura and N. Kosugi, J. Electr. Spectrosc. Rel. Phen. **177** (2010) 130.

BL3U

Development of a Microfluidic Cell for Soft X-ray Absorption Spectroscopy

M. Nagasaka[1], H. Fischer[2], H. Yuzawa[1], M. Nakano[1], N. Takada[1], M. Aoyama[1], E. Rühl[2] and N. Kosugi[1]

[1]*Institute for Molecular Science, Okazaki 444-8585, Japan*
[2]*Physikalische Chemie, Freie Universität Berlin, Takustr. 3, D-14195 Berlin, Germany*

Microfluidics is a chemical technique to realize highly efficient chemical reactions in liquids and solutions [1]. Recently, X-ray diffraction in the hard X-ray region has been used for a variety of systems by using microfluidics [2]. However, it is difficult to apply spectroscopic techniques in the soft X-ray region since soft X-rays cannot penetrate a microfluidic cell. In this study, we have successfully measured fluorescence excitation spectra resembling soft X-ray absorption spectroscopy (XAS) of structured liquids by developing a microfluidic cell with a 100 nm thick SiC membrane window.

The experiments were performed at BL3U connected to a developed microfluidic cell. A T-shape microfluidics setup with the width of 50 μm is made from PDMS resin which is covered by a 100 nm thick SiC membrane. The adhesion of PDMS to the SiC membrane is realized by pressing a Si frame of the membrane with O-rings. Pyridine and water are mixed in the T-shape microfluidics cell with flow rate of 10 μL/min by using syringe pumps. The microfluidic cell is placed in a helium in atmosphere. The ultrahigh vacuum of the soft X-ray beamline is separated from the microfluidic cell by a 100 nm thick SiC membrane with a window size of 36 × 23 μm^2, which determines the soft X-ray beam size. Spatially resolved XAS spectra of microfluidic cell are measured in the fluorescence mode by using a silicon drift detector.

Figure 1 shows a soft X-ray fluorescence image of the T-shape microfluidic cell excited by soft X-rays at 550 eV. The fluorescence image shows high intensity due to water, since the excitation energy of 550 eV is above the O K-edge. Water flows from the upper side, and pyridine from the lower side. The water-pyridine mixture flows to the right hand part after the junction of the liquids. Figure 2 shows N K-edge XAS spectra of microfluidic cell at different positions. The N 1s → π* peak of pyridine in the mixed position (X=350, Y=200) shows a shift to higher photon energy than is observed for pure pyridine at X=200, Y=100. The energy shift of the pyridine-water mixture is consistent with our previous XAS studies [3], in which the formation of a hydrogen bond of the N atom in pyridine with water causes a shift to higher photon energy of the π* peak.

We have successfully measured spatially resolved XAS of microfluidics in the soft X-ray regime with a spatial resolution of 36 × 23 μm^2. In the future, we will investigate several chemical reactions occurring in microfluidic cell by spatially resolved XAS using our T-shape microfluidics setup.

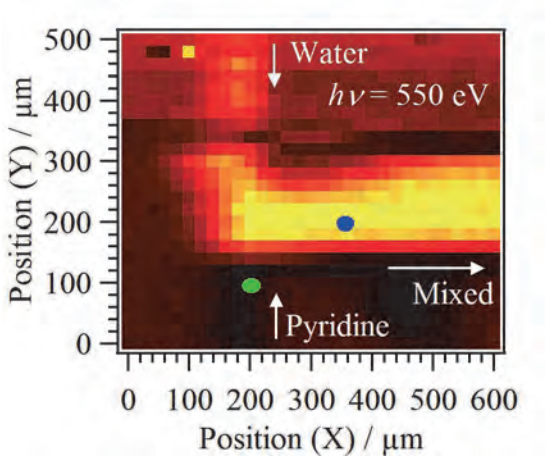

Fig. 1. Soft X-ray fluorescence image of a T-shape microfluidic cell excited by soft X-rays at 550 eV. The flows of pyridine and water are mixed in this device. It also shows two spots to measure N K-edge XAS spectra, as shown in Fig. 2.

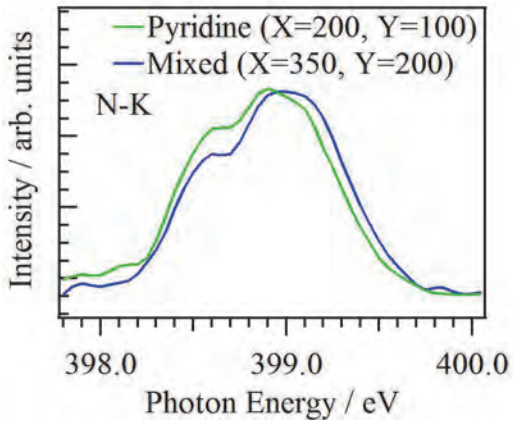

Fig. 2. N K-edge XAS spectra at different positions in the T-shaped microfluidic cell at positions indicated in Fig. 1.

[1] T. Kitamori *et al.*, Anal. Chem. **76** (2004) 53.
[2] B. Weinhausen and S. Köster, Lab Chip **13** (2013) 212.
[3] M. Nagasaka *et al.*, J. Electron Spectrosc. Relat. Phenom. **200** (2015) 293.

BL4U

Characterization of Macroporous Monolithic Polymers Containing Amphiphilic Macro-RAFT Agent by Scanning Transmission X-Ray Microscopy (STXM)

D. Arrua[1], A. Khodabandeh[2], T. Ohigashi[3], N. Kosugi[3] and E. Hilder[1]

[1]*Future Industries Institute, University of South Australia, Building X, Mawson Lakes Campus, GPO Box 2471 Adelaide SA 5001, Australia*

[2]*Australian Centre for Research on Separation Science (ACROSS), School of Chemistry, University of Tasmania, Private Bag 75, Hobart 7001, Australia*

[3]*UVSOR Facility, Institute for Molecular Science, Okazaki 444-8585, Japan*

Macroporous polymer materials with interconnected structures represent a useful class of polymers used in different fields including separation science in the last decades [1]. An increasingly exploited method for the preparation of highly porous scaffolds is based on the solidification of the continuous phase of a high internal phase emulsion (HIPE) through polymerization. A cellular monolithic structure, commonly with interconnected pores and hence an open cellular network is produced, referred to as a poly(HIPE). Our aim here is to develop a surfactant-assisted functionalization strategy for preparation of styrene-based porous polymers by HIPE polymerization, whereby the obtained porous polymers have a specific application [2]. An accurate characterization of such polyHIPE material is needed to better understand the polymer morphology as well as surface chemistry [3].

The characterization by STXM of polyHIPE materials was performed at the BL4U beamline of the UVSOR synchrotron radiation facility. STXM imaging was conducted by focusing on the C 1s core-line signal in NEXAFS. Fig. 1 shows the C 1s NEXAFS spectra obtained for both polyHIPEs (A1 with macro-RAFT agent and A2 with End-group removed macro-RAFT agent) cross-linked styrene network.

The components found by STXM were the poly(Sty-co-DVB) polyHIPE, the macro-RAFT agent, and the embedding resin. The spectrum for the crosslinked styrene-based scaffold has a strong peak at 284.6 eV, which is characteristic of C 1s → π*C=C transition in a phenyl ring. The macro-RAFT agent spectrum shows two peaks: a strong peak at 284.9 eV, which corresponds to the C 1s → π*C=C transition of the phenyl ring (styrene of macro-RAFT agent) and a peak at 288.9 eV, which is characteristic of C 1s → π*C=O transition in esters. Using a sequence of highly resolved X-ray photon energies covering the C 1s spectral region (280 to 320 eV), successive image was obtained for polyHIPE A2. STXM composite component map on polyHIPE respect to the corresponding X-ray spectra of references, the macro-RAFT agent, Styrene-DVB crosslinked polymer network and epoxy components are shown in blue, green, and red, respectively in Fig. 2.

As a conclusion, soft X-ray microscopy images recorded at multiple wavelengths have been used to qualify the chemical composition in polyHIPE. The results shown in this work clearly demonstrate how STXM analysis can reveal chemical information for these materials.

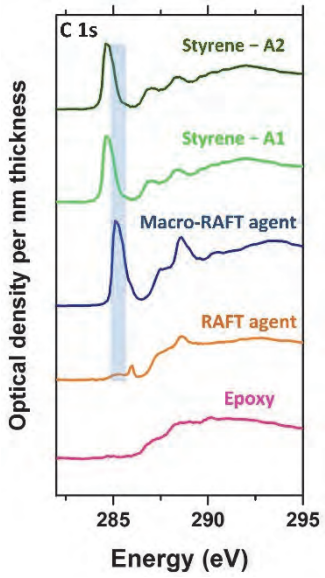

Fig. 1. NEXAFS reference spectra of the epoxy (embedding matrix), RAFT agent, macro-RAFT agent, and polystyrene cross-linked polyHIPEs that correspond to 1 nm thickness of each component.

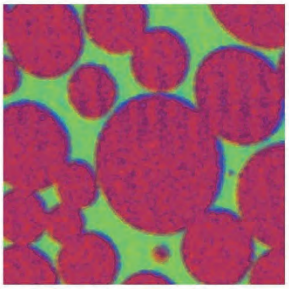

Fig. 2. STXM color coded composite map (red=epoxy, green=PSty, blue=macro-RAFT agent).

[1] D. Wu *et al.*, Chem. Rev. **112** (2012) 3959.
[2] A. Khodabandeh *et al.*, Poly Chem **7** (2016) 1803.
[3] D. Arrua *et al.*, UVSOR Activity Reports **42** (2014) 76.

BL4U

Liquid-Liquid Interface between Triethylamine and Water Phases Studied by Spatially-Resolved Soft X-ray Absorption Spectroscopy

M. Nagasaka, T. Ohigashi, H. Yuzawa, Y. Inagaki and N. Kosugi
Institute for Molecular Science, Okazaki 444-8585, Japan

Aqueous triethylamine (TEA) solution shows a lower critical solution temperature (LCST) behavior [1], in which two liquids are mixed at the lower temperature and splits into two phases with the temperature increase. Because the phase transition is contrary to normal, the mechanism of LCST has not yet been fully understood. In this study, we have investigated local structures of liquid-liquid interfaces between TEA and water phases by spatially-resolved soft X-ray absorption spectroscopy (XAS).

The experiments were performed using a liquid flow cell in STXM (scanning transmission X-ray microscope) on BL4U [2]. The liquid layer is sandwiched between 100 nm-thick Si_3N_4 membranes. The liquid-liquid interface between TEA and water phases is formed from aqueous TEA solutions with the molar fraction of 0.4 at the temperature of 29.9 ºC, which is above the LCST.

Figure 1 shows O K-edge XAS of water at different positions of the liquid-liquid interfaces. The inset shows the soft X-ray transmission image at 530 eV, in which the center part is a water phase and is surrounded by a TEA phase. We have measured O and C K-edge XAS in the region indicated by the red arrow. Figure 2 shows molar concentrations of water and TEA at different positions, which is determined from the edge-jumps of XAS in O and C K-edges, respectively. In the TEA phase, the molar fraction of TEA is increased to 0.6 because water molecules are gathered to the water phase. It is consistent with the phase diagram of TEA-water mixtures [1], where the LCST is increased at the higher fraction of TEA. In the liquid-liquid interface, on the other hand, the amount of TEA is reduced to one third, and that of water is drastically increased. In the water phase, the most part is water molecules due to the formation of hydrogen bonding (HB) network of water.

Figure 3 shows the energy shifts of the pre-edge peaks (535 eV) in the O K-edge XAS at different positions. It is already known that the pre-edge peak is shifted to the lower photon energy when HB between water molecules is elongated. From the water to the TEA phase, the pre-edge peaks show lower energy shifts. Because the amount of water is decreased with the direction of the TEA phase, the hydrophobic interaction of ethyl group in TEA is stronger than the HB interaction of water, which leads to the elongation of the HB network. Water and TEA molecules are coexisted in the TEA phase because the HB network of water is weakened. The liquid-liquid interface between water and TEA phases is formed with the balance of the hydrophobic interaction of TEA and HB interaction of water, which is changed by gathering water molecules to the water phase.

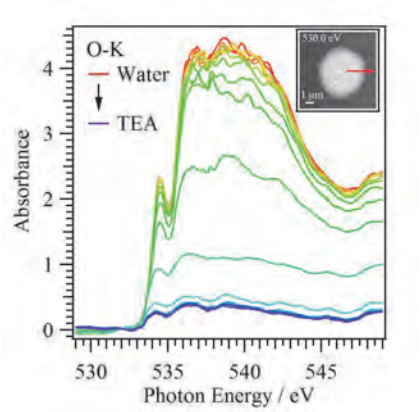

Fig. 1. O K-edge XAS of water at different positions. The inset shows the image at 530 eV, in which the red arrows indicate the measurement region.

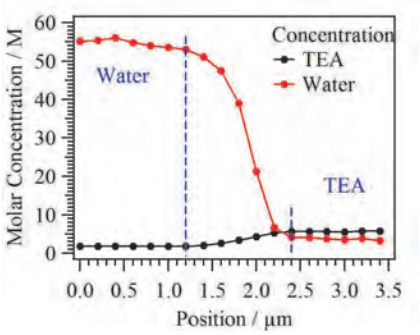

Fig. 2. Molar concentration of liquid-liquid interface determined from the edge-jump of XAS.

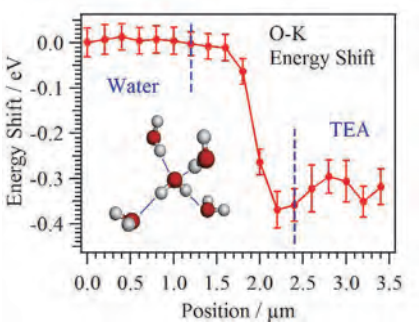

Fig. 3. Peak shift of the pre-edge peak in O K-edge XAS as a function of positions in the liquid-liquid interface.

[1] F. Kohler and O. K. Rice, J. Chem. Phys. **26** (1957) 1614.
[2] T. Ohigashi *et al.*, AIP Conf. Proc. **1741** (2016) 050002.

BL4B

Photoelectron-Auger Electron Coincidence Study of the Electron Emission from Condensed Water Molecules

R. Mashiko[1], K. Soejima[1], E. Shigemasa[2] and Y. Hikosaka[3]

[1]*Department of Environmental Science, Niigata University, Niigata 950-2181, Japan*

[2]*UVSOR Facility, Institute for Molecular Science, Okazaki 444-8585, Japan*

[3]*Graduate School of Medicine and Pharmaceutical Science, University of Toyama, Toyama 930-0194, Japan*

Electron coincidence spectroscopy enables one to clarify energy correlations between electrons emitted after a single photon. Extremely-efficient electron coincidence measurements can be achieved by a use of the magnetic bottle technique [1]. In the present study, photoelectron-Auger electron coincidence spectroscopy using a magnetic bottle electron spectrometer is applied to the study of inner-shell photoionization of water molecules condensed on solid surface [2].

The experiment was performed at the beamline BL4B under the single bunch operation of the storage ring. Water molecules were adsorbed on the surface of a copper wire, by continuously cooling the wire down to the liquid nitrogen temperature, under the base pressure of ~1.8×10^{-8} Torr. Coincidence datasets were accumulated with a magnetic bottle electron spectrometer [3], for electrons emitted from the condensed water on irradiation of 738.2 eV photons.

The two-dimensional map in Fig. 1 displays the energy correlation of the coincident electrons included in the coincidence datasets. A clear structure running vertically is associated with the coincidences between the O1s photoelectrons and the Auger electrons from condensed water. To display the O1s photoelectron structure closely, the coincidence counts on the map are projected onto x-axis and are presented in the top panel. The projection curve shows an O1s photoelectron peak displaying a continuous structure on the lower kinetic energy side. The long tail is attributed mainly to the photoelectrons with reduced energies due to inelastic scatterings on the escape from the inside of the water condensation.

Figure 2 presents Auger electron spectra observed in coincidence with O1s photoelectrons (region (a) in Fig. 1) and energy-loss photoelectrons due to inelastic scatterings (region (b) in Fig. 1). The coincidence Auger spectrum in Fig. 2 (a) shows a considerable intensity below 420 eV, which is ascribable to an energy loss of the Auger electrons due to the inelastic scattering. In Fig. 2 (b), the contribution from the inelastic scattering is enhanced. This observation can be understood as follows: the selection of photoelectrons with energy loss picks out the photoemission events for H_2O molecules distant from the outermost surface and thus the Auger electrons ejected from these molecules are also subject to remarkable inelastic scattering.

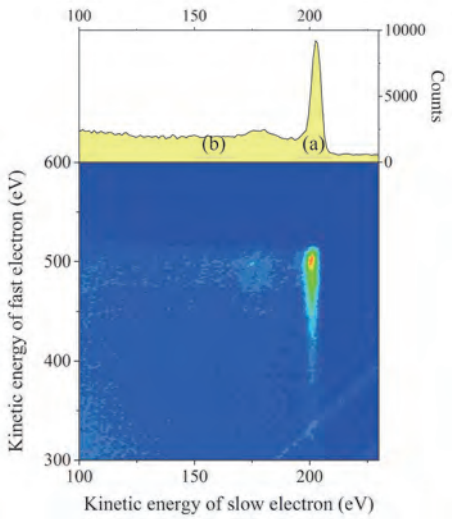

Fig. 1. Two-dimensional map showing the energy correlation of the coincident electrons emitted from condensed water molecules on irradiation of 738.2 eV photons.

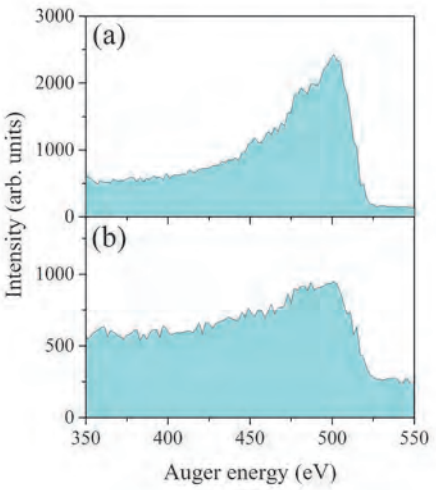

Fig. 2. Auger electron spectra observed in coincidence with O1s photoelectrons (region (a) in Fig. 1) and energy-loss photoelectrons due to inelastic scatterings (region (b) in Fig. 1).

[1] J. H. D. Eland *et al*., Phys. Rev. Lett. **90** (2003) 053003.
[2] Y. Hikosaka *et al*., J. Electron Spectrosc. Rel. Phenom. **213** (2016) 17.
[3] Y. Hikosaka *et al*., J. Electron Spectrosc. Rel. Phenom. **192** (2014) 69.

BL6U

Producing Mechanism of Metastable OCS^{3+} Studied by Photo-Electron-Ion Coincidence Method

F. Kumaki[1], H. Iwayama[2], E. Shigemasa[2] and K. Soejima[1]
[1]*Department of Environmental science, Niigata University Niigata 950-2181, Japan*
[2]*UVSOR Facility, Institute for Molecular Science, Okazaki 444-8585, Japan*

We have studied that dissociation processes and stabilities of molecules absorbed a soft X-ray which are photo-ionized and subsequently lead to Auger decay. While most multicharged molecular ions produced after photo-ionization immediately dissociate due to the Coulomb repulsion, the existence of metastable multicharged molecular ions depending on the electronic states is known. As a few exceptions, producing processes of the metastable multicharged molecular ions are almost not clarified. The OCS molecule is known to produce a doubly-ionized molecular ion. In the past work, we studied the processes of the producing metastable OCS^{2+} by an Auger electron-photo ion coincidence technique. The observation was done for Auger decay from C1s, O1s and S2p inner shell photoionization. The valence electronic configuration of the OCS is described as $(6\sigma)^2(7\sigma)^2(8\sigma)^2(9\sigma)^2(2\pi)^2(3\pi)^2$. This measurement revealed that metastable OCS^{2+} can be produced when its Auger final states with the $(3\pi)^{-2}$ configuration. Also it was revealed that metastable OCS^{2+} produced following S2p photoionization is populated with much higher possibility compared with that arising from C1s and O1s photoionizations. It is understood that the origin of this site-specificity in the production of metastable OCS^{2+} arises from the spacial distribution of 3π valence orbital involved [1, 2]. It is also known that the metastable triply-ionized OCS molecule exists. Does theproduction mechanism of the metastable OCS^{3+} have characters like that of metastable OCS^{2+}? In this work, we have studied metastable OCS^{3+} by the photoelectron-photoion coincidence measuremens.

The experiment was performed at the beamline 6U of the UVSOR facility. We used the electron-ion coincidence spectrometer consisting of a double toroidal electron analyzer and an ion time-of-flight (TOF) analyzer [2]. We measured photoelectronphotoion coincidence signals following C1s, O1s and S2p photoionization.

Figure 1 shows TOF spectra of photoions arising from Auger decay following C1s, O1s and S2p photoionization respectively in coincidence with the photo-electrons. The peaks of OCS^{3+} are commonly observed around 2500 ns though these are weak. The ratio of the coincidence counts of C1s, O1s and S2p photoionization is C1s:O1s:S2p = 2.8:1:1.9. The ratio in metastable OCS^{2+} is S2p > O1s > C1s in the past experiment. The result of OCS^{3+} is different from that. This indicates the existence of site-specificity in the production metastable OCS^{3+} different from that in the production of metastable OCS^{2+}. In the future experiment, we will observe using an Auger electron - photoion coincidence method.

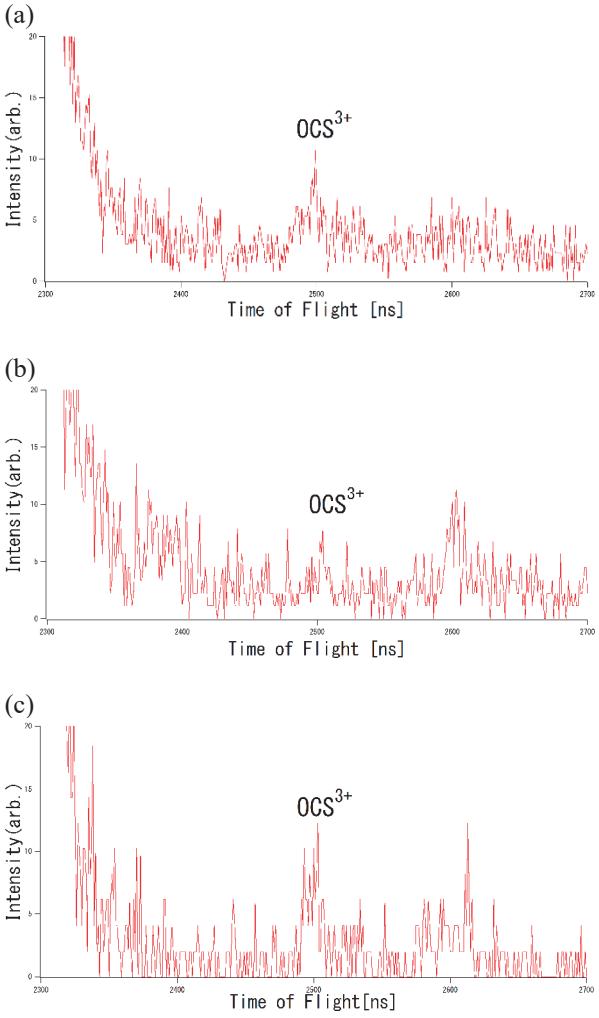

Fig. 1. TOF spectra of ions produced by Auger decay following C1s, O1s and S2p ionization in coincidence with photo-electron. (a) C1s ionization (b) O1s ionization (c) S2p ionization.

[1] T. Kaneyasu *et al*., J. Korean Phys. **54** (2009) 371.
[2] T. Kaneyasu *et al*., J. Phys. B: At. Mol.Opt. Phys. **48** (2015) 125101.

BL6U

F KVV and Xe $M_{45}N_{45}N_{45}$ Auger Spectra of Xenon Difluoride across the Xe 3d and F 1s Thresholds

F. Yamashita[1], M. Kono[2, 3, 4], H. Iwayama[5, 6], K. Okada[1] and E. Shigemasa[5, 6]

[1]*Department of Chemistry, Hiroshima University, Higashi-Hiroshima 739-8526, Japan*
[2]*Senri International School of Kwansei Gakuin, Minoh 562-0032, Japan*
[3]*School of Science and Technology, Kwansei Gakuin University, Sanda 669-1337, Japan*
[4]*RSPE, Australian National University, Canberra, ACT 2601, Australia*
[5]*UVSOR Facility, Institute for Molecular Science, Okazaki 444-8585, Japan*
[6]*School of Physical Sciences, The Graduate University for Advanced Studies (SOKENDAI), Okazaki 444-8585, Japan*

Xenon difluoride has been of great interest as a noble gas compound. The molecule intrigues X-ray spectroscopists because it has similar binding energies among Xe $3d_{5/2}$, Xe $3d_{3/2}$ and F 1s subshells [1]. Southworth *et al.* recently measured the partial ion yield curves of XeF_2 and found that the charge state distribution of Xe^{q+} shifts down compared to the Xe atom case [2]. This report focuses on the Auger spectroscopy in order to get more insight into the molecular electronic states leading to the production of Xe^{q+}. Resonant and normal Auger spectra are acquired as a function of photon energy in this study.

The experiments were performed on the soft X-ray beamline, BL6U. A main chamber was equipped with a gas cell and a high-resolution hemispherical electron analyzer (MBS A-1). Sublimated XeF_2 sample was introduced into the cell so as to keep the pressure in the main chamber at 7.5×10^{-4} Pa during the measurements. The electron spectra were acquired over the photon energy range of 668.9–709.9 eV. The energy resolutions of incident photons and detected electrons were set at 0.7 and 0.48 eV, respectively.

Figure 1 shows typical resonant and normal Auger spectra plotted on the electron kinetic energy scale. The peaks labeled A–E can be assigned to the Auger transitions of F KV_oV_o, F KV_iV_o, F KV_iV_i, Xe $M_4N_{45}N_{45}$ and Xe $M_5N_{45}N_{45}$, respectively, referring to the Auger spectra of Xe [3] and F_2 [4]. Here the symbols V_o and V_i represent outer- and inner-valence orbitals, respectively. The photon energy of 682.9 eV corresponds to the resonance transition from Xe $3d_{3/2}$ and/or F 1s to the σ^* orbital. Figure 1 reveals that the Auger band A is most intense at this resonance, indicating that the F 1s excitation is dominant and thereby suggesting that the Auger final states have two holes in the V_o orbital(s) plus an electron in the σ^* orbital. This is consistent with the study by Southworth *et al.*, reporting the specific increase in the Xe^+ and F^+ ion yields at the σ^* resonance [2]. At the photon energy of 686.7 eV, on the other hand, which is assigned to the shape resonance, Xe $3d_{5/2}^{-1}\epsilon f$, the Auger band E (Xe $M_5N_{45}N_{45}$) is predominantly observed. This transition is followed by the cascade Auger processes where ionization repeats until the holes are left in the valence orbitals. The occurrence of these processes is consistent with the fact that the branching ratios of multi-charged Xe^{2+}, Xe^{3+} and Xe^{4+} ions increase [2]. Our results illustrate that a strong correlation exists between the Auger transitions and fragmentation channels. We have a plan to carry out the Auger-electron–photoion coincidence (AEPICO) measurements to justify this directly and the results will be published in the near future.

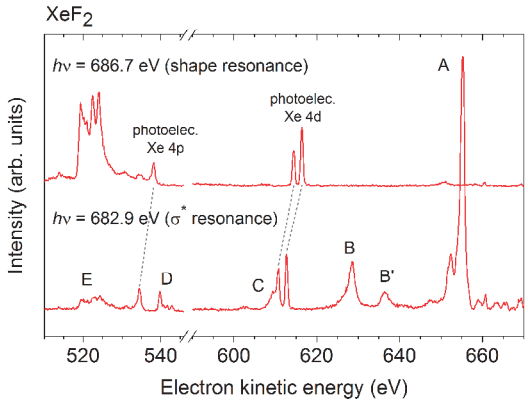

Fig. 1. Resonant and normal Auger spectra of xenon difluoride. A, F KV_oV_o; B and B′, F KV_iV_o; C, F KV_iV_i; D, Xe $M_4N_{45}N_{45}$; and E, Xe $M_5N_{45}N_{45}$. The dotted lines show the peak correspondence for the Xe 4p and 4d photoelectrons.

[1] T. X. Carroll, R. W. Shaw Jr., T. D. Thomas, C. Kindle and N. Bartlett, J. Am. Chem. Soc. **96** (1974) 1989.
[2] S. H. Southworth, R. Wehlitz, A. Picón, C. S. Lehmann, L. Cheng and J. F. Stanton, J. Chem. Phys. **142** (2015) 224302.
[3] L. O. Werme, T. Bergmark and K. Siegbahn, Phys. Scr. **6** (1972) 141.
[4] P. Weightman, T. D. Thomas and D. R. Jennison, J. Chem. Phys. **78** (1983) 1652.

BL6U

Formation of H_2^+ Fragments in Dissociation of Methanol Dication

M. Higuchi[1], K. Soejima[1], H. Iwayama[2], E. Shigemasa[2] and Y. Hikosaka[3]

[1]*Department of Environmental Science, Niigata University, Niigata 950-2181, Japan*
[2]*UVSOR Facility, Institute for Molecular Science, Okazaki 444-8585, Japan*
[3]*Graduate School of Medicine and Pharmaceutical Sciences, University of Toyama, Toyama 930-0194, Japan*

When a molecule absorbs a soft x-ray photon, inner-shell photoionization emitting a photoelectron are induced and then Auger decay emitting an Auger electron follows. Because two electrons are emitted through this process, the molecule with two positive charges, or molecular dication, is produced. The dication dissociates into ion pairs due to the Coulomb repulsion between the two positive charges. In this study, we have investigated the dissociation fragments from dication states formed after the inner-shell photoionization and the Auger decay process of methanol molecules.

The experiment was performed in the undulator beamline BL6U at the UVSOR facility. We used an electron-ion coincidence spectrometer composed of a toroidal electron analyzer and an ion momentum imaging analyzer.

In this report, we focus on the formation of molecular hydrogen ion from dication states in methanol molecule. Fig. 1 shows time-of-flight spectra of light fragment ions produced after the C1s inner-shell ionization of CH_3OH (black), CD_3OD (green), CH_3OD (red) and CD_3OH (blue). In the three panels, the spectra for the individual deuterated methanol molecules are compared with the one for CH_3OH. The formation of H_2^+ fragments is observed in the CH_3OH spectrum, where the fragments can be produced from two hydrogen atoms originally bonded to the C atom, or from one hydrogen atom at the C side and the hydrogen atom at the O side. The intensity of D_2^+ in the CD_3OD spectrum is about the half of H_2^+ in the CH_3OH spectrum, which manifests that deuteration reduces the formation of molecular hydrogen ion from the dication states.

When only the hydrogen atom at the O side is deuterated (i.e., for CH_3OD), the HD^+ formation, as well as the intense H_2^+ peak, is weakly observed. This observation implies that, while the molecular hydrogen ions are mainly from the hydrogen atoms at the C side, a fraction of the molecular hydrogen ions is produced from one hydrogen atom at the C side and the hydrogen atom at the O side. On the other hand, formation of HD^+ is hardly identified in the CD_3OH spectrum; the HD^+ formation using the hydrogen atoms at both sides is reduced by the deuteration at the C side. This finding suggests that the hydrogen migration forming HD^+ is mainly from the C side to the O side, and the migration is discouraged by the deuterium of hydrogen atoms at the C side.

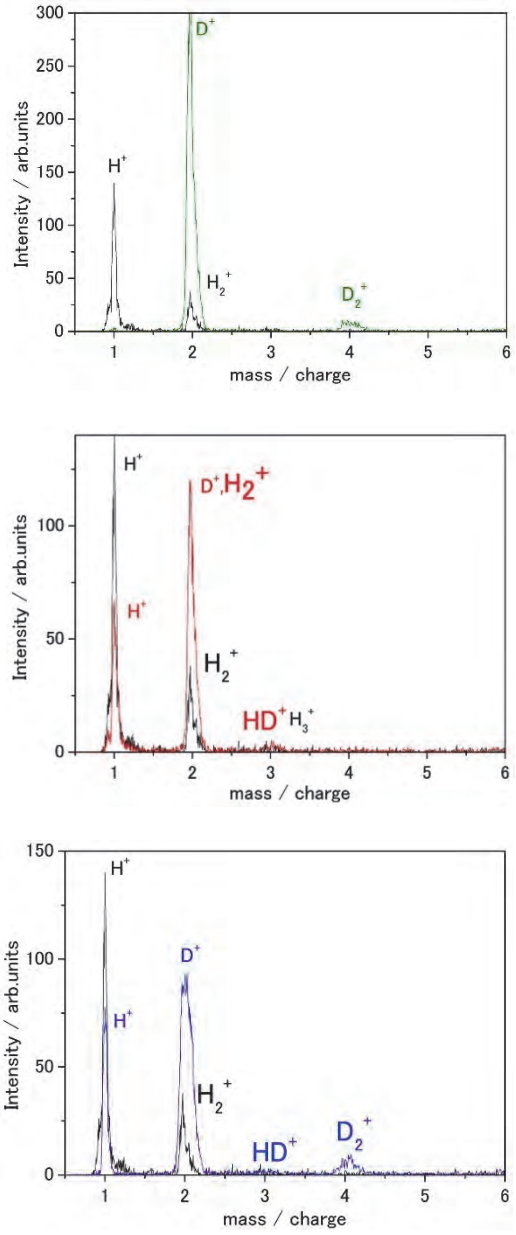

Fig. 1. Time-of-flight spectra for CD_3OD (green), CH_3OD (red) and CD_3OH (blue), compared with the time-of-flight spectrum for CH_3OH (black).

BL6U

Dissociation Dynamics of Dication States in Water Molecules

F. Kumaki[1], K. Soejima[1], H. Iwayama[2], E. Shigemasa[2] and Y. Hikosaka[3]

[1]*Department of Environmental science, Niigata University Niigata 950-2181, Japan*

[2]*UVSOR Facility, Institute for Molecular Science, Okazaki 444-8585, Japan*

[3]*Graduate School of Medicine and Pharmaceutical Sciences, University of Toyama, Toyama 930-0194, Japan*

A molecule absorbed a soft X-ray photon may lead to inner shell ionization and subsequently to Auger decay. Emission of two electrons through this sequential process results in the production of a doubly-ionized molecule. The doubly-ionized molecule called dication is unstable because of the Coulomb repulsion of two plus charge in the molecule, and often becomes fragmentation into ion pairs. In this work, we have studied the dissociation processes of dication states in water molecules by an electron-ion coincidence method.

The experiment was performed at the beamline 6U of the UVSOR facility. We used the electron-ion coincidence spectrometer consisting of a double toroidal electron analyzer and an ion time-of-flight (TOF) analyzer [1]. We measured Auger electron-ion coincidences for the gas-phase H_2O, D_2O and HDO to understand the deuteration effect in the dissociations of the dication states.

The black curves in Fig. 1 are the Auger spectra of H_2O and D_2O, which show band structures. The coincidence Auger spectra filtered for the two-body fragmentations into H^++OH^+ or D^++OD^+ are represented in red, and those filtered for the three-body fragmentations into H^++O^++H or D^++O^++D are in blue. The peaks of the two-body fragmentations and three-body fragmentations are commonly observed around 41eV and 45eV, respectively. In both H_2O and D_2O, the two-body dissociation is preferred to the three-body dissociation. The ratios of the coincidence counts for the two-body and the three-body dissociations are 1.9:1 for H_2O and 3.1:1 for D_2O; the contribution from the three-body dissociation is higher in H_2O than in D_2O [2].

Figure 2 shows the two-dimensional TOF map of ion pairs formed after the Auger decay in HDO, observed in coincidence with Auger electrons in the whole energy range. Two structures indicated by circles correspond to two-body dissociations of $HDO^{2+}\rightarrow H^+$-OD^+ and $HDO^{2+}\rightarrow D^+$-OH^+. The intensity ratio of the two dissociations is estimated, from the coincidence counts in the map, to be H^+-OD^+ : D^+-OH^+ = 2.3:1. The elongation of the D-O bond takes longer in time than that of the H-O bond because of the heavier hydrogen atom, which may results in the favorable dissociation of the H-O bond.

(a)

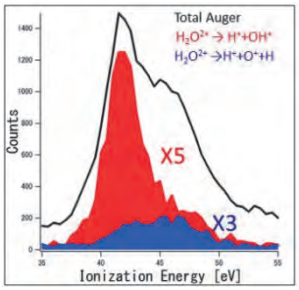

(b)

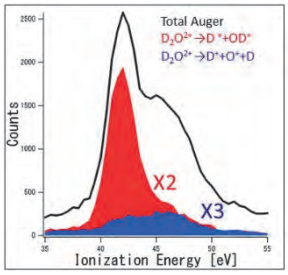

Fig. 1. Total Auger spectra (black) and coincidence Auger spectra filtered for the two-body dissociation (red) and for the three-body dissociation (blue) in (a) H_2O and (b) D_2O [2].

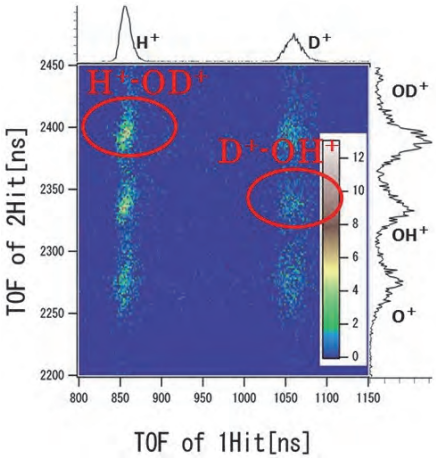

Fig. 2. Two-dimensional TOF map of ion pairs following HDO Auger decay observed in coincidence with Auger electrons in the whole energy range.

[1] T. Kaneyasu *et al*., J. Phys. B: At. Mol. Opt. Phys. **48** (2015) 125101.

[2] M. Kikuchi *et al*., UVSOR Act. Rep. **43** (2016) 106.

BL6U

Chemical Shift of Inner-Shell Binding Energies in Primary Bromoalkanes

H. Fujise[1, 2], H. Iwayama[1, 2] and E. Shigemasa[1, 2]

[1]*Institute for Molecular Science, Okazaki 444-8585, Japan,*

[2]*School of Physical Sciences, The Graduate University for Advanced Studies (SOKENDAI), Okazaki 444-8585, Japan*

Molecular inner-shell electrons do not play significant roles in forming chemical bonds, however, studies suggest that there are differences in the inner-shell binding energy for an atom of certain elements, depending on the chemical environments of the probed atom. This is called a "chemical shift". Remarkable chemical shifts of inner-shell binding energies of the carbon 1s electron in four different bonding environments of ethyl trifluoroacetate have been successfully demonstrated by Siegbahn [1]. To elucidate the molecular size effects of these chemical shifts on inner-shell ionization energies and binding energies of Auger final states, we have measured the Br 3d photoelectrons and MVV (V = valence level) Auger electrons produced after inner-shell photoionization in primary bromoalkanes.

The experiment was conducted on the soft X-ray beamline BL6U at UVSOR. The radiation from the undulator was monochromatized by a variable included angle varied line-spacing plane grating monochromator. The monochromatized light was introduced into a gas call with the sample gas mixture ($CH_3(CH_2)_nBr$ (n = 0 - 6): 90%, Kr: 10%). The photon energies for 3*d* photoelectron and Auger electron measurements were set to 200 eV, and 88 eV, respectively. The kinetic energies of the emitted electrons were measured by a hemispherical electron energy analyzer (MBS-A1), at a magic angle of 54.7° from the polarization vector. The resolution of the kinetic energy depends on the pass energy of the electrons in the hemisphere, and the width of the entrance slit of the analyzer, which were set to ~30 meV and ~6 meV, at pass energies 50 and 10 eV, respectively, at a slit width of 0.2 mm. The kinetic energy scales were calibrated with the 3*d* and 4*s* photoelectrons of Kr atoms in the sample gas mixture, for 3*d* photoelectron and Auger electron measurements, respectively.

The Br 3*d* photoelectron spectra of $CH_3(CH_2)_nBr$ (n = 0 - 6) are shown in Fig. 1. Two broad structures observed for all n, are assignable to the Br $3d_{3/2}$ and $3d_{5/2}$ components. In practice, it is known that the broad structures are attributed to the total of five ligand field splitting peaks [2], furthermore, there were no differences observed between the position of the ligand-field splitting components and molecular size. The broad structures shift to the lower binding energy side, as the molecular size increases. These chemical shifts imply that the charge distribution of bromoalkanes are different in size, and may be attributed to factors such as the different electronegativities of larger ligands. The Auger spectra for CH_3Br and $C_7H_{15}Br$ are shown in Fig. 2. The peak profile of the spectra become more complex as the number of carbon atoms increase in the alkane chain, and the kinetic energies shifts to the higher energy side. This is attributed to the more complex molecular orbitals and electronic structures involved in the MVV Auger process observed.

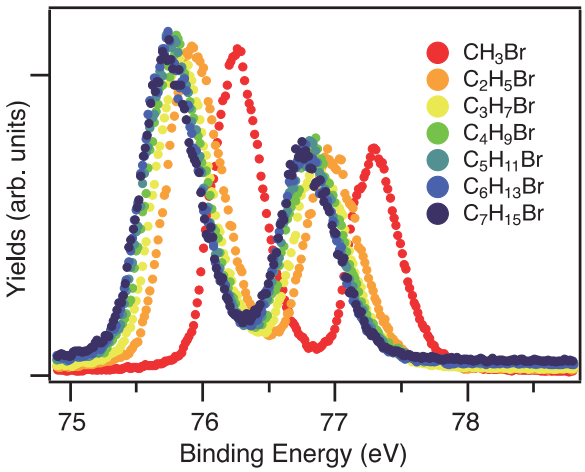

Fig. 1. Photoelectron spectra of $CH_3(CH_2)_nBr$ (n = 0 - 6) measured at photon energies 200 eV.

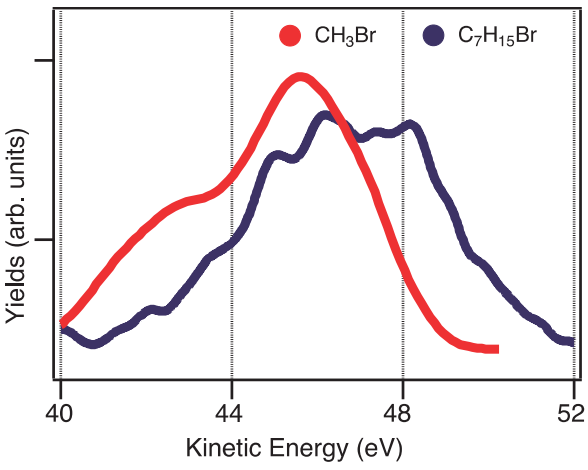

Fig. 2. Auger spectra of $CH_3(CH_2)_nBr$ (n = 0 ~ 6) measured at photon energies 88 eV.

[1] K. Siegbahn, Pure & Appl. Chem. **48** (1976) 77.
[2] J. Johnson *et al.*, J. Phys. B: At. Mol. Opt. Phys. **30** (1997) 4899.

BL6U

Intermolecular Vibrational Relaxations of Core Excited Nitrogen Clusters

H. Iwayama[1, 2] and E. Shigemasa[1,2]

[1]*UVSOR Facility, Institute for Molecular Science, Okazaki 444-8585, Japan*
[2]*School of Physical Sciences, The Graduate University for Advanced Studies (SOKENDAI), Okazaki 444-8585, Japan*

The photoreaction of isolated molecules in the gas phase is one of the most studied chemical reactions. However, since most chemical reaction in nature take place in condensed matter such as solids and liquids, it is important to understand intermolecular processes. Photodissociation of molecules in condensed matter would be quite different from that of isolated molecules, since energy and charge transfers into neighboring molecules may suppress molecular dissociation. Mass measurements of fragment ions in condensed matter are desirable, but it is difficult to extract them from solids or liquids. On the other hand, molecules in clusters have a similar environment to condensed matter, and their fragments can be easily measured as well as isolated molecules. In this work, we performed Auger-electron-ion coincidence measurements for isolated nitrogen and clustered nitrogen and investigated intermolecular processes of core excited nitrogen clusters.

The Auger-electron-ion coincidence measurements were performed on the undulator beamline BL6U at UVSOR. The Auger electrons and product ions were measured in coincidence by a double toroidal electron analyzer (DTA) and an ion momentum spectrometer, respectively. The pass energy of DTA was set to 400 eV. All signals from the ion and electron delay-line detectors were recorded with an 8ch TDC board. The photon energy was tuned to 401.1 eV, which corresponds to the resonance energy of the N 1s $\rightarrow\pi^*$ excitation for isolated and clustered nitrogen[1]. Nitrogen clusters were produced by supersonic expansion through a 100-μm nozzle at 110 K. The average cluster size was estimated to be ~300 molecules per cluster.

Figure 1 shows time-of-flight mass spectra for (a) molecular nitrogen and (b)clustered nitrogen. For molecular nitrogen, we observed parent molecular ions of N_2^+ and fragment ions of N^+. For clustered nitrogen, we observed $(N_2)_n^+$ ($n \geqq 1$) and $(N_2)_nN^+$ ($n \geqq 0$). In the present condition, the abundance of N^+ ions from core excited nitrogen clusters was negligibly small.

Figure 2 shows the coincidence Auger spectra for (a)isolated and (b)clustered nitrogen. Most N_2 molecules dissociate into N^+ fragment ions above 23.4 eV, which is corresponds to the lowest dissociation limit of N_2^+. This is because isolated molecules can release the excess energy only by radiative decays, whose time scales are nanoseconds, much slower than that of the dissociation process. On the other hand, for clustered nitrogen, we observed significant amount of N_2^+ ions well above the N_2^+ dissociation limit. This may suggest that intermolecular process, such as, vibrational relaxations suppress molecular dissociation. Analysis in more detail is in progress.

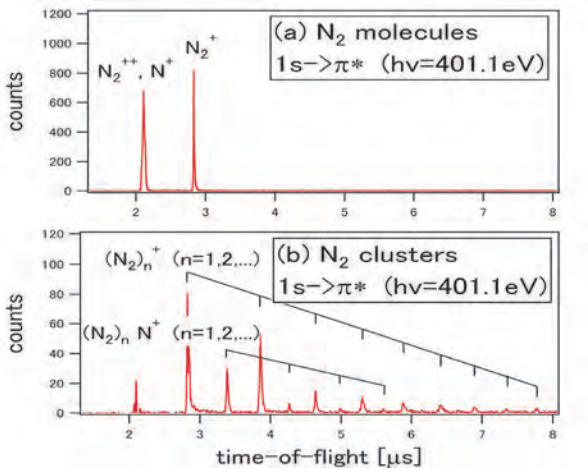

Fig. 1. Time-of-flight mass spectra for (a) N_2 molecules and (b) clusters. For nitrogen clusters, we subtracted contributions of molecular nitrogen in the cluster beam.

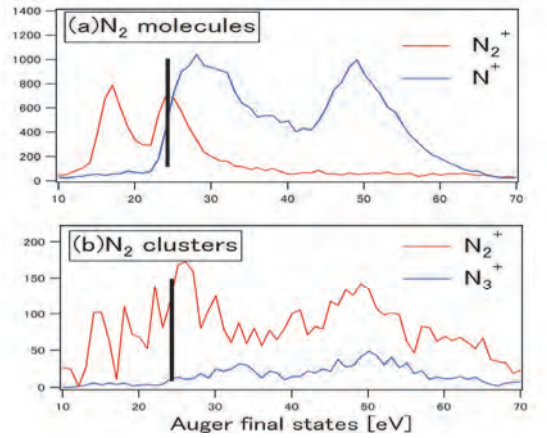

Fig. 2. Coincidence Auger spectra for (a)N_2 molecules and. (b)clusters. For nitrogen clusters, we subtracted contributions of molecular nitrogen in the cluster beam. Black bars represents the lowest dissociation limit of N_2^+.

[1] R. Flesch *et al.*, Phys. Rev. Lett. **86** (2001) 3767.

BL6B

Infrared Microscopy of Pyridine-Water Mixtures in T-Shape Microfluidics

M. Nagasaka[1], H. Fischer[2], H. Yuzawa[1], M. Nakano[1], N. Takada[1], M. Aoyama[1], E. Rühl[2] and N. Kosugi[1]

[1]*Institute for Molecular Science, Myodaiji, Okazaki 444-8585, Japan*
[2]*Physikalische Chemie, Freie Universität Berlin, Takustr. 3, D-14195 Berlin, Germany*

Microfluidics is a chemical technique to realize highly efficient chemical reactions in liquids and solutions [1]. Recently, X-ray diffraction in the hard X-ray region has been used for a variety of systems by using microfluidics [2]. On the other hand, we have developed a microfluidic system for soft X-ray absorption spectroscopy (XAS) [3]. In this study, we have used it for infrared (IR) microscopy.

The experiments were performed by using the IR microscopy setup IRT-7000 at UVSOR BL6B. A T-shape microfluidics setup with the width of 50 μm is made from PDMS resin which is covered by a 100 nm thick Si_3N_4 membrane. Pyridine and water are mixed in the T-shape microfluidic cell with a flow rate of 20 μL/min by using syringe pumps. The spatial resolution of 30 × 30 μm^2 is reached by using a ×16 Cassegrain mirror. IR spectra are taken by detecting the reflected infrared light with an MCT detector.

Figure 1(a) shows an optical microscopic image of the T-shape microfluidic cell. Water and pyridine are flowed in the left and right hand parts, respectively. We have found a laminar flow, in which pyridine and water are separately flowed at the center of the mixing region behind the junction of the liquids. Figure 1(b) shows IR spectra of pyridine and water taken from the microfluidic system. The IR spectra show the OH stretching vibration of water at 3507 cm^{-1} and the CH stretching vibration of the pyridine ring around 3100 cm^{-1}, respectively. We have measured IR spectra with a spatial resolution of 30 × 30 μm^2 in the same region of the optical image shown in Fig. 1(a). The absorbance of pyridine and water at different positions is obtained by fitting the IR spectra to the mentioned vibrational peaks of pyridine and water.

Figure 1(c) shows the 2D image of the absorbance of pyridine. The right hand part and the mixed region of the T-shape microfluidic cell show high intensity of pyridine. The left hand part of the laminar flow in the mixed region, which is mainly filled with water, also shows high intensity of pyridine. Because the spatial resolution of the IR microscope (30 × 30 μm^2) is larger than the width of the pyridine part in the laminar flow (25 μm), the water part in the laminar flow also shows some intensity of pyridine. Figure 1(d) shows a 2D image of the absorbance of water. Unlike the pyridine case, water shows high intensity outside the microfluidic channel. This means that the adhesion of the Si_3N_4 membrane to PDMS was insufficient in the water part, which is unlike the pyridine part. Recently, we have measured XAS of pyridine-water mixtures in our T-shape microfluidic system, and confirmed the adhesion of SiC is sufficient even in the water part [3]. Note that the microfluidic cell is kept in a helium atmosphere, where the pressure is several percent higher than the ambient pressure. The adhesion of SiC to PDMS is then strong enough because the SiC membrane is pressed by the helium gas. In the future, we will include this helium pressing system to the microfluidic cell in order to take more reliable IR microscopy images of T-shape microfluidics.

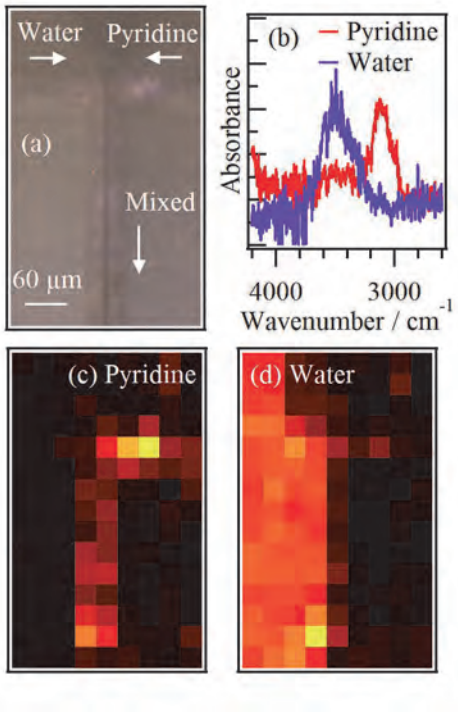

Fig. 1. (a) An optical microscopy image of the T-shape microfluidic cell. A laminar flow is formed after mixing the flows of pyridine and water. (b) IR spectroscopy of pyridine and water taken from the positions of pyridine and water in T-shape microfluidic cell. The 2D images of the absorbance of (c) pyridine and (d) water in the T-shape microfluidic cell are also shown.

[1] T. Kitamori *et al.*, Anal. Chem. **76** (2004) 53.
[2] B. Weinhausen and S. Köster, Lab Chip **13** (2013) 212.
[3] M. Nagasaka *et al.*, in this volume.

UVSOR User 6

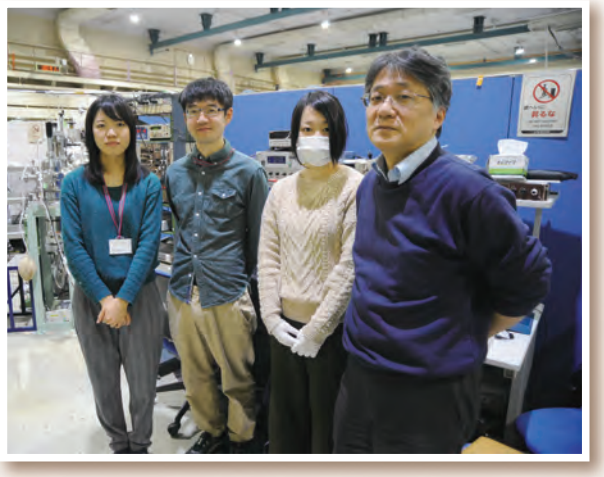

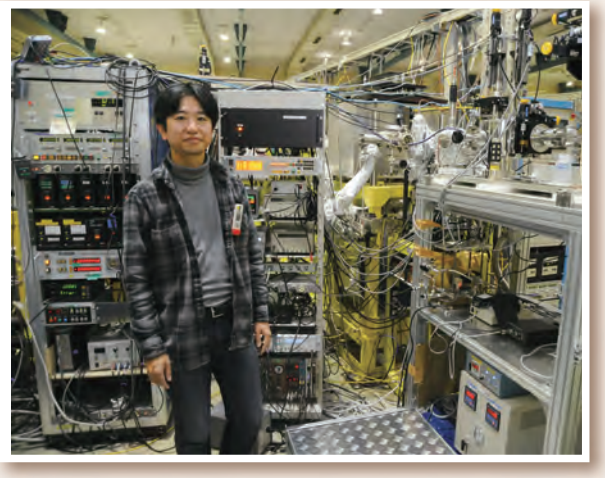

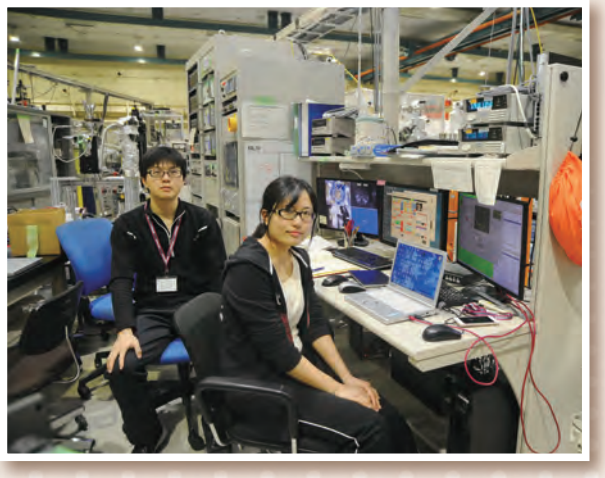

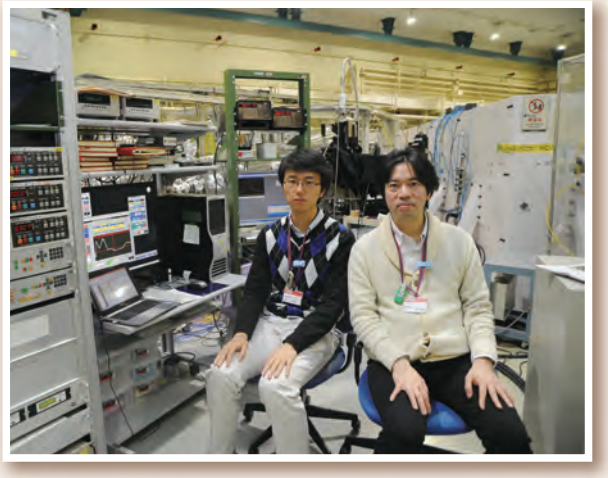

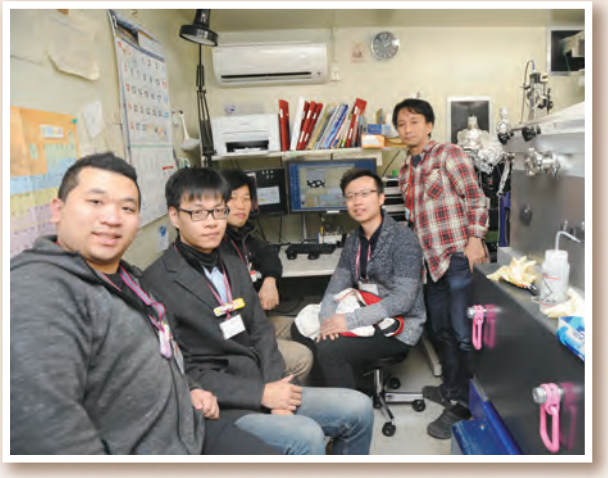

UVSOR User 7